Ethylene-vinyl acetate copolymer/aluminium trihydroxide composites: A new method to predict the barrier effect during cone calorimeter tests

Florian Cavodeau, Rodolphe Sonnier, Belkacem Otazaghine, José-Marie Lopez-Cuesta, Christelle Delaite

HAL Id: hal-02914224

https://hal.science/hal-02914224

Submitted on 23 May 2022

Ethylene-vinyl acetate copolymer/aluminium trihydroxide composites: A new method to predict the barrier effect during cone calorimeter tests

Florian Cavodeau [a], Rodolphe Sonnier [a], Belkacem Otazaghine [a, *],
José-Marie Lopez-Cuesta [a], Christelle Delaite [b]

[a] Centre des Matériaux des Mines d'Alès (C2MA), 6 Avenue de Clavières, 30319 Alès Cedex, France
[b] Laboratoire de Photochimie et d'Ingénierie Macromoléculaire (LPIM), 3bis Rue Alfred Werner, 68100 Mulhouse, France

ABSTRACT

This study presents the use of oedometric compression test in order to evaluate the breakdown of a protective layer acting as a diffusion barrier ("barrier effect") occurring during cone calorimeter tests for ethylene-vinyl acetate copolymer/aluminium trihydroxide (EVA/ATH) composites. The formation of an alumina layer at the sample surface during burning insulates thermally the underlying material and reduces the heat release rate. The efficiency of this barrier depends on the cohesion of the layer formed. This cohesion depends on the ability of the particles (ATH and synergistic mineral fillers) to self-arrange. During the test, the breakdown of this barrier can lead to an increase in HRR.

The oedometric compression test allows assessing the ability of fillers to form a cohesive layer. Results obtained from compression modulus of filler powders are directly related to some aspects of the heat release rate curve of composites measured in cone calorimeter tests. Indeed, the appearance and the intensity of the second pHRR (related to the breakdown of the barrier layer) in cone calorimeter test are related to the slope of oedometric compression curve.

1. Introduction

Due to their properties and processing characteristics, ethylene-vinyl acetate (EVA) copolymers are commonly used in the wire and cable industry. However, these polymers are easily flammable, so flame retardant (FR) systems have to be introduced during the process [1]. In EVA copolymers, hydrated mineral fillers, such as alumina trihydroxide (ATH) and magnesium dihydroxide (MH) are widely used in fire retardancy systems at very high loadings (up to 65 wt%).

The interest of hydrated mineral fillers (hydroxides and hydroxycarbonates) is mainly based on the following fire retardant mechanisms, described below [2]:

Dilution of the solid combustible fraction; endothermic decomposition of the filler; dilution of fuels in gaseous phase; formation of a protective barrier.

The efficiency of hydrated mineral fillers on fire retardancy depends on the amount of released molecules, on the related enthalpy of reaction and on the temperature range of filler decomposition. For example, ATH decomposes into boehmite at 180−200 °C, releasing two molecules of water. Then, the boehmite formed decomposed at higher temperature (500−550 °C), leading to alumina with the release of a third molecule of water. The whole decomposition absorbs 1.3 kJ/g, as an endothermic reaction [3].

The barrier effect is then provided by the alumina and depends on the organisation of the particles at the surface of the polymer [4]. It seems that a compact layer of inert fillers leads to a more efficient insulation from the heat and also restricts the diffusion of fuels into the flame. A model proposed by Staggs also confirms this observation [5]. The efficiency of this barrier can be improved by the presence of synergistic additives, which helps the formation of a cohesive structure [6−9]. Moreover, geometric characteristics such as particle size, aspect ratio and size distribution of alumina particles could play an essential role on the organisation of the protective layer [10].

The effect of the particle size of hydrated fillers was studied, regarding the relative efficiency in fire retardancy tests [11]. In a

previous study, carried out at our laboratory, it was shown that a better flame resistance can be reached by using a combination of different particles sizes [12]. This result was due to a more compact organisation of particles.

Represented as spheres, a packing of monodisperse particles presents voids between them, in which smaller particles can intercalate [10].

Benezet et al. showed that the shape of particles is a major parameter regarding the compactness and the compressibility of a powder sample [13]. A bimodal distribution theoretically leads to a more compact packing at the surface of the burning polymer. This packing can be estimated by a compression test, forcing the particles to reach the optimal organization [14,15].

Concerning the barrier effect due to a packing of inorganic fillers, Hshieh et al. worked on deposited silica-ash layer in silicones [16]. In this work, silica-ash samples of different thicknesses were placed on a sensor, under the cone calorimeter. The authors showed that the presence of a barrier effect due to the organisation of particles improves the fire resistance of materials.

In the present study, an adapted oedometric method was used [17]. The oedometric compression is a method generally used for the analysis of soils in civil engineering [17,18]. In the present case, a uniaxial compression at constant speed was used to measure the vertical tension during the test and the maximum resistance of the sample toward the force applied. This resistance is closely related to the deformation of the sample along the axe of compression.

We assumed that the resistance during an oedometric compression for a heterogeneous mixture of particles can be related to its optimum packing, and so its ability to form a cohesive layer during a fire test. Cone calorimetry was widely used to investigate the mechanisms of action of fire retardants. Both physical and chemical effects are taken into account using this device. The barrier effect can be visualized, on cone calorimeter curves, by a gradual decrease of the heat release rate after a first peak. A longer decrease corresponds to a more efficient barrier effect [19]. The protective role of the barrier effect is disrupted when the cracking of the layer occurs. This is represented on cone calorimeter curves by an increase of the heat release rate, i.e. a second peak.

2. Experimental

2.1. Materials

The EVA copolymer used was a thermoplastic-elastomeric grade Alcudia® PA-440 (Repsol), with a melt flow index of 7 g/10min (190 °C, 2.16 kg) and a vinyl acetate content of 28 wt%. Aluminium trihydroxides (ATH) were supplied by Alteo (SH15, SH20, SH100 and SH30N) and Albemarle (OL-104 LEO), with various particle size distribution, aspect ratio and specific surface area. SH20, SH100 and OL-104 LEO are precipitated ATH, with a pseudo-spherical shape. SH15 and SH30N are grinded ATH, with a platelet shape. Median diameters (D_{50}) were determined by laser diffraction.

Some silica-based synergistic agents were selected: two non-

commercial grades of crushed diatomite (raw and calcined) and a spherically-shaped amorphous silicon dioxide supplied by Elkem (Sidistar® T-120). Some major characteristics are presented in Table 1. The calcination of diatomite was made during 1 h at 1000 °C under air [20]. Calcination of diatomite led to an internal sintering [21], entailing a decrease of the porosity and internal surface, and hence of the global surface area. This was confirmed by S_{BET} measurements presented in Table 1.

Powder true density was measured using a helium pycnometer AccuPyc 1330 (Micromeritics). Specific surface area (S_{BET}) was measured by N_2 adsorption at 77 K (BET method), using an SA 3100 analyser (Beckman−Coulter). Particle size (D_{50}) was measured in water with a laser diffraction particle size analyser LS 13320 (Beckman−Coulter), using an ultrasonic device to break particles agglomerates. Main characteristics of the fillers are given in Table 1.

2.2. Processing

Processing was carried out by incorporating the fillers into EVA using a twin-screw extruder (Clextral BC21, 900 mm) at 160 °C and then pressed using an injection moulding machine (Krauss-Maffei 50T-KM50/180CX). Sheets of $100 \times 100 \times 4$ mm^3 were prepared at 140 °C under a pressure of 100 bars. Table 2 summarizes all the formulations prepared. The total filler content was 60 wt% for each formulation. Only sample 14 contains 45% of fillers due to the volume restriction of the twin-screw extruder.

2.3. Characterizations

Flammability was studied using a cone calorimeter (Fire Testing Technology - FTT) according to the ISO 5660 standard (sample dimensions $100 \times 100 \times 4$ mm^3). External heat flux was set to 50 kW/m^2. The variations of Heat Release Rate (HRR), peaks of Heat Release Rate (pHRR), time to pHRR (tpHRR) and Total Heat Release (THR) were measured. In this study, the second part of the curve (specifically the second peak of HRR related to the breakdown of the barrier layer, pHRR2) was scrutinized (see Fig. 1).

The theoretical mass loss of samples was measured by thermogravimetric analysis (TGA), using a Pyris 1 TGA (Perkin Elmer). The analyses were made under air, from 20 to 900 °C at 10 °C/min.

An adapted two-piston oedometric compression cell was designed (Fig. 2). A mass of 10 g of product was introduced in the cell for each test. The two-piston system was chosen for easier sample release and cleaning. A classic oedometric test uses a non-deformable compression cell, in which the sample is introduced. In the present case, the smaller piston acts as the bottom of the compression cell, and will not move during the test. The force is applied by means of the bigger piston. The compression was carried out using a Z010 Material Testing Equipment (Zwick) with a 10 kN sensor, at a speed of 10 mm/min. The procedure was validated by reproducibility tests.

A schematic representation of the uniaxial oedometric compression test is shown in Fig. 3.

Table 1
Characteristics of fillers.

Filler	Denomination	Powder true density (g/cm^3)	S_{BET} (m^2/g)	D_{50} Laser (μm)	Mineral composition
SH15	A1	2.48	20.58	1.7	$Al(OH)_3$
SH20	A2	2.45	3.93	2.1	$Al(OH)_3$
SH100	A3	2.44	2.94	10.3	$Al(OH)_3$
SH30N	A4	2.51	10.61	2.8	$Al(OH)_3$
OL-104 LEO	A5	2.52	4.76	1.9	$Al(OH)_3$
Sidistar®T-120	S1	2.24	19.22	0.2	SiO_2
Crushed diatomite (raw)	S2	2.17	23.43	2−5	SiO_2
Crushed diatomite (calcinated)	S3	2.37	13.71	2−5	SiO_2

Table 2
List of formulations.

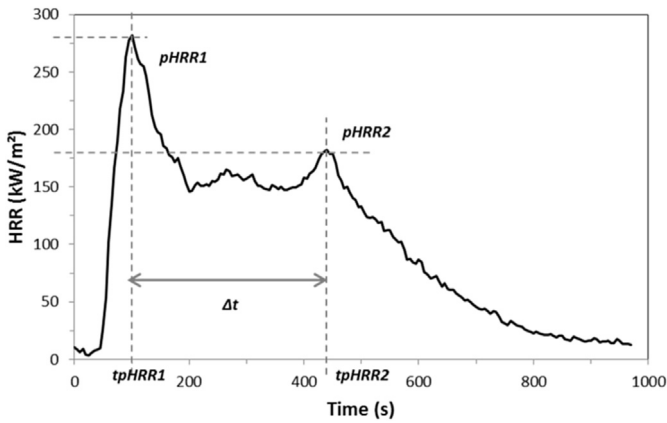| Formulation	EVA (wt%)	SH15 (wt%)	SH20 (wt%)	SH100 (wt%)	SH30N (wt%)	OL-104 (wt%)	T-120 (wt%)	Diatom (raw) (wt%)	Diatom (calcinated) (wt%)
1: 60A1	40	60	–	–	–	–	–	–	–
2: 60A2	40	–	60	–	–	–	–	–	–
3: 60A3	40	–	–	60	–	–	–	–	–
4: 60A4	40	–	–	–	60	–	–	–	–
5: 60A5	40	–	–	–	–	60	–	–	–
6: 54A2/6A3	40	–	54	6	–	–	–	–	–
7: 30A2/30A3	40	–	30	30	–	–	–	–	–
8: 12A2/48A3	40	–	12	48	–	–	–	–	–
9: 50A2/10S1	40	–	50	–	–	–	10	–	–
10: 50A2/10S3	40	–	50	–	–	–	–	–	10
11: 55A2/5S2	40	–	55	–	–	–	–	5	–
12: 50A2/10S2	40	–	50	–	–	–	–	10	–
13: 45A2/15S2	40	–	45	–	–	–	–	15	–
14: 45S2	55	–	–	–	–	–	–	45	–
15: EVA	100	–	–	–	–	–	–	–	–

Fig. 1. A typical HRR curve with two peaks of heat release rate.

F represents the force applied by the piston, S the surface of the sample, h_0 the initial thickness of the sample, Δh the difference between the initial and final thicknesses, σ_y the strain along the y axis and $\varepsilon_y/\varepsilon_x/\varepsilon_z$ the deformation along each axis.

This test allowed us to obtain a typical compression curve (shown in Fig. 4), in which the variation of the force applied on the sample can be measured. The curve obtained represents the variation of thickness of the sample versus the compression force. As the piston progresses along the cell, the powder is packed and the particles self-organize, leading to a maximum packing allowed by the limit of the 10 kN sensor.

Two domains are observed on the typical compression curve, corresponding to two different slopes. The first step corresponds to a rough organisation of the particles, in which the air is progressively released, leading to a more compact system. The second step corresponds to a higher resistance to compression of the particles, with a forced re-organization due to the compression.

The slope of the first part of each curve is slightly the same for all fillers (σ^*). On the contrary, a variation can be noticed for the estimated percentage of compression (%C) and the slope of the second part (σ). This slope is calculated on a linear section of the second part of the curve:
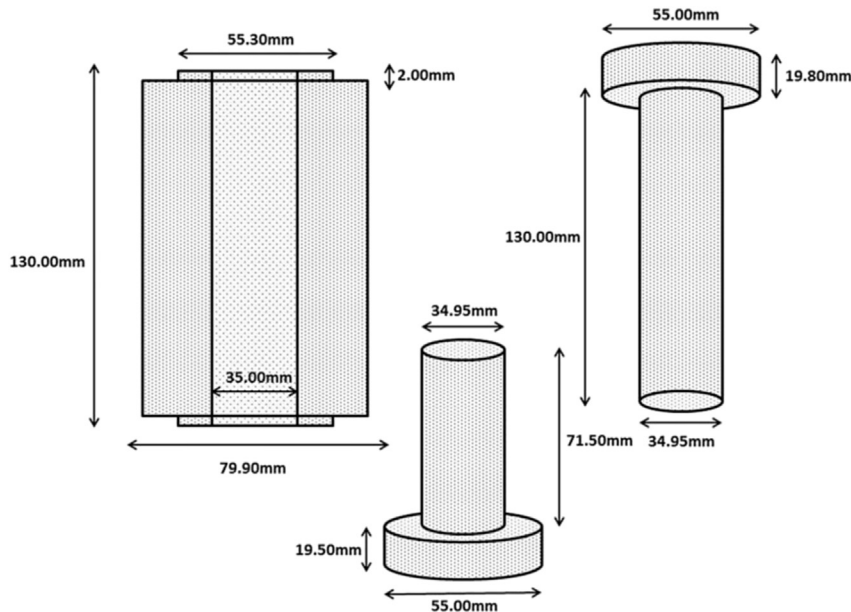
$$\sigma = \frac{y_{max} - y_{min}}{x_{max} - x_{min}}$$

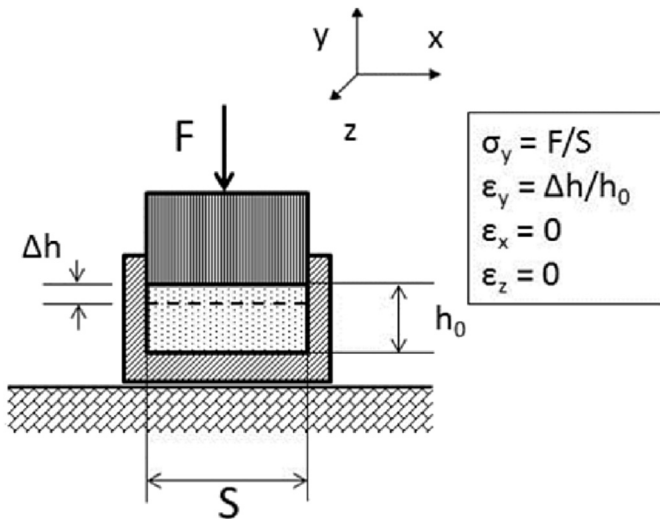**Fig. 2.** A two-piston oedometric compression cell.

Fig. 3. A representation of the oedometric compression.

$$\sigma_y = F/S$$
$$\varepsilon_y = \Delta h/h_0$$
$$\varepsilon_x = 0$$
$$\varepsilon_z = 0$$

Fig. 5. Laser diffraction analysis of SH100 after different forces of compression (on fillers).

A laser diffraction analysis was carried out to control the size of particles after a compression test. Indeed, the compression may break aggregates and thereby modifies the size distribution of the sample. As an example, size analysis results obtained with SH100 for compression of 0 kN, 5 kN, and 10 kN are presented below (Fig. 5).

Only the disappearance of a peak at 600 µm corresponding to particles agglomerates can be observed. As expected, compression does not seem to break primary particles.

Differences between each size distribution appear to be essentially a consequence of a de-agglomeration due to the compression. The same tendency was noticed with other samples.

3. Results & discussion

3.1. Cone calorimeter tests

All results are presented on Table 3, including Time To Ignition (TTI), first peak of Heat Release Rate (pHRR1), corresponding time (tpHRR1), second peak of Heat Release Rate (pHRR2), corresponding time (tpHRR2), Total Heat Release (THR), and Mass Loss. Calculated mass loss is determined by TGA analysis, to estimate the maximum residue rate theoretically present at the end of the cone calorimeter test. This mass loss was determined by calculation, based on the content of fillers for each sample and the mass loss
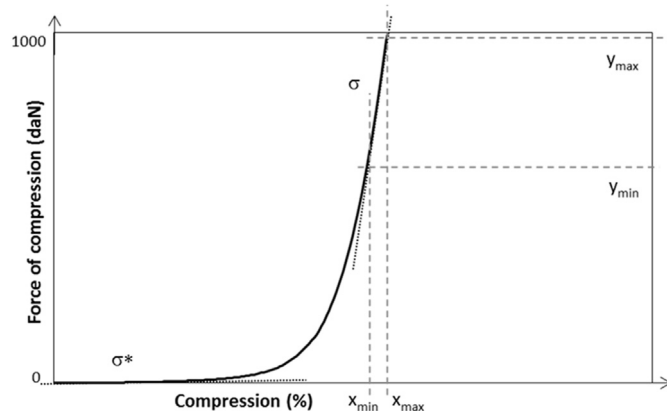

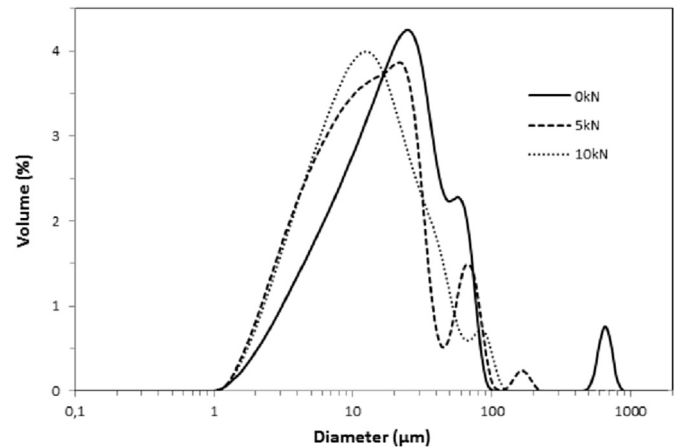**Fig. 4.** A schematic compression curve and related parameters.

due to the release of gases of decomposition, measured by TGA. Regarding TGA results of the fillers, mass loss reaches 34.4% for A1, 34.0% for A2, 34.2% for A3, 34.1% for A4 and 33.7% for A5. Mass loss for S1, S2 and S3 is 0%. A comparison with the effective mass loss, measured during cone calorimeter tests, enables to estimate the residue rate. Time between pHRR1 and pHRR2 is also presented (Δt). Results presented in Table 3 are average values of cone calorimeter tests, based on three measurements for each formulation.

The results of cone calorimeter test on formulations containing only ATH (1−5) show that particle size and shape of the filler modify the fire behavior of the composite. Fig. 6 presents HRR curves for these formulations. As the median diameter decreases from 10 µm to 2 µm, pHRR1 is reduced of about 70 kW/m^2 and pHRR2 of about 40 kW/m^2. Furthermore, the second peak is delayed of 100 s. For the formulation 3, a third peak appears during the test, probably due to the lack of stability of the layer formed during the fire. Results in Table 3 confirm that formulation 3 presents the less efficient barrier effect. Concerning the shape of particles, a comparison between formulation 4 and formulation 5 shows that the presence of pseudo-spherical particles leads to a higher pHRR1 and to an earlier and higher pHRR2. Moreover, the ignition is slightly delayed, as the pHRR1. It is well known that particles with a high aspect ratio, such as platelets, impart a better fire reaction and a better barrier effect [22,23]. Disparity of results between sample 2 and sample 5, with particle of close median diameters, may be explained by the difference of polydispersity indexes. Further experiments are needed to clarify this assumption. SEM images of compared particles are presented on Fig. 7.

Concerning the formulations containing particles of median diameter of 10 and 2 µm (formulations 6 to 8), the results confirm that the presence of smaller particles in the composite improves the flame retardancy (Fig. 8). Indeed, formulation 6, with the largest amount of small particles (54 wt%), presents lower pHRR1 and pHRR2, and this last peak appears later.

Even a small amount of particles of median diameter of 10 µm in the mixture deteriorates the properties compared to formulation 2. The results confirm that the use of one size distribution with a low D$_{50}$ provides a better flame retardancy.

Formulations 9 to 14 contain between 5 and 45% of silica-based synergistic agents. It has been shown that the presence of a small quantity of silica particles [7] improves the fire retardancy in EVA compositions. It seems that silica-particles act as a thermal stabilizer, help the intumescence process but decrease the char cohesion. The effect is more noticeable for silica particles of high specific

Table 3
Results of cone calorimeter tests.

Formulation	TTI (s)	pHRR1 (kW/m²)	tpHRR1 (s)	pHRR2 (kW/m²)	tpHRR2 (s)	Δt (s) (tpHRR2-tpHRR1)	THR (kJ/g)	Mass loss (%)	Calculated Mass loss (%)
1: 60A1	49	221.37	110	123.58	580	470	15.00	59.6	60.9
2: 60A2	43	207.96	102	137.81	540	438	18.02	59.6	60.5
3: 60A3	40	271.03	105	190.98	445	340	19.93	60.4	60.7
4: 60A4	57	212.32	125	104.82	657	532	14.02	58.0	60.7
5: 60A5	64	257.39	140	160.5	545	405	14.12	60.1	60.5
6: 54A2/6A3	45	251.12	117	151.62	530	413	15.78	59.7	60.9
7: 30A2/30A3	50	276.60	102	178.23	492	390	15.83	58.9	60.5
8: 12A2/48A3	46	282.04	97	183.13	467	370	15.22	59.4	60.5
9: 50A2/10S1	54	241.95	125	104.12	652	527	14.34	58.4	57.6
10: 50A2/10S3	56	221.39	100	91.72	701	601	12.99	57.8	57.7
11: 55A2/5S2	46	198.51	92	87.12	742	650	15.06	57.7	59.0
12: 50A2/10S2	54	151.78	112	66.74	832	720	11.33	50.6	57.8
13: 45A2/15S2	54	144.89	107	87.89	747	640	12.18	47.6	56.0
14: 45S2	29	667.98	80	237.43	355	275	23.40	53.5	54.7
15: EVA	37	810.23	230	—	—	—	23.62	100	100

surface area. Regarding its analogy with silica-based porous structures, diatomite (or diatomaceous earth) was incorporated as a potential synergistic agent. The calcinated version of the diatomite and silica particles were used for a comparison of the influence of the porous structure of fillers on fire properties of composites. Indeed, as the fillers presented the same amorphous structure of SiO_2, differences on flame retardancy may be due to the geometric structure, the roughness, the specific surface area and the porosity or the size distribution of particles. Results are presented in Fig. 9.

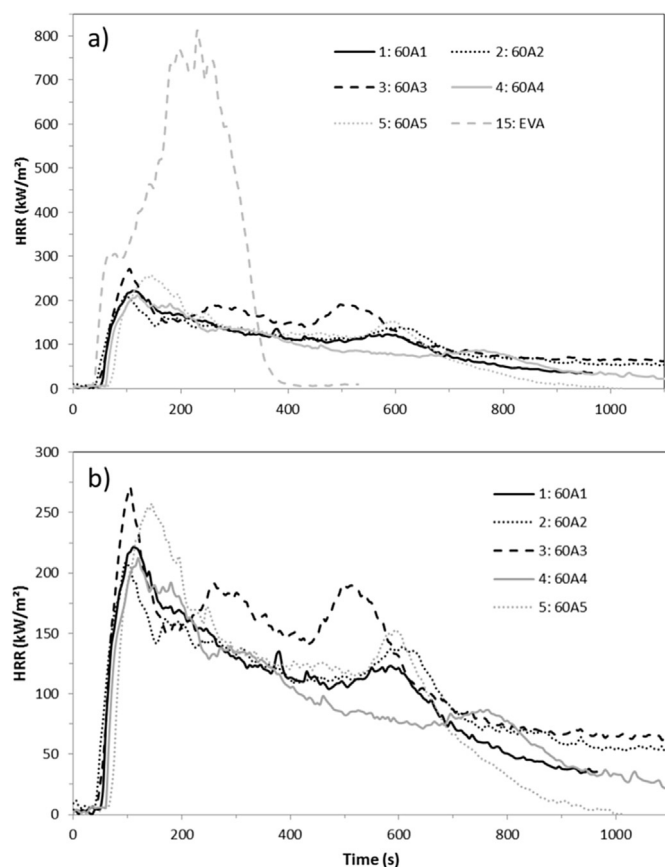Without ATH, formulation 14 (filled with 45% of crushed

Fig. 6. HRR curves: Effect of different ATH (formulations 1 to 5) and comparison with pure EVA (formulation 15). All curves (a) and zoom without pure EVA (b).

diatomite) is not efficiently flame retarded. It presents a high pHRR1 of almost 670 kW/m² with an ignition at 30 s. The presence of ATH seems to be essential for the efficiency of the flame retardancy. However, the decrease of the heat release rate, following by the apparition of a second pHRR, confirms the formation of a relatively resistant barrier layer.

For this series, 2 μm ATH were chosen (A2). The action of this filler reduces the pHRR1 in each case. Formulation 10 (with 50% of ATH and 10% of calcinated diatomite) and formulation 11 (with 55% of ATH and 5% of raw diatomite) present a pHRR1 equivalent to that of the formulation containing only ATH A2 (formulation 2). Nevertheless, both pHRR2 are lower than 100 kW/m², evidencing a more resistant barrier layer. Formulation 9 (with 50% of ATH and 10% of silica particles), presents also a cohesive barrier layer (about 100 kW/m² for pHRR2), but an increased pHRR1 (240 kW/m²) compared to formulation 2. All these formulations form a complex foamed residual structure (Fig. 10). This structure is less developed for samples 9 (with 10% of silica particles) and 10 (with 10% of calcinated diatomite), with a less intense swelling during cone calorimeter tests.

With 10% of raw diatomite, the pHRR1 is reduced to 150 kW/m² and to 145 kW/m² with 15% of this filler. However, the barrier effect seems to be better for the formulation filled with 10% of raw diatomite (formulation 12) than the sample with 15% of raw diatomite (formulation 13). pHRR2 of formulation 13 is equivalent to pHRR2 of formulation 11, even if pHRR1 of formulation 13 is lower by 50 kW/m².

Visually, the swelling is more intense for formulation 13 during the cone calorimeter test but the cracking of the protective layer occurs earlier than the one for formulation 12, with less diatomite. A hypothesis would be that pyrolysis gases are more retained underneath the burning surface, due to a more resistant structure for formulation 13, increasing the pressure. So, even if the barrier layer seems to be more resistant for formulation 13 than for formulation 12, a higher pressure of gases may force the barrier to break, leading to an earlier pHRR2.

It can be noticed that formulations presenting the more important swelling (formulations with 5, 10 and 15% of raw diatomite), also present a larger gap between the mass loss measured during the cone calorimeter test, and the calculated theoretical mass loss (see Table 3). This gap increases with the amount of diatomite in the formulation; it reaches 1.3% for the formulation with 5% of diatomite, 7.2% for the formulation with 10% and 8.4% for the formulation with 15% of raw diatomite. Regarding these observations, it can be suggested that the formation of an expanded structure during fire testing could prevent the polymer from degrading completely. It seems that a certain amount of residual
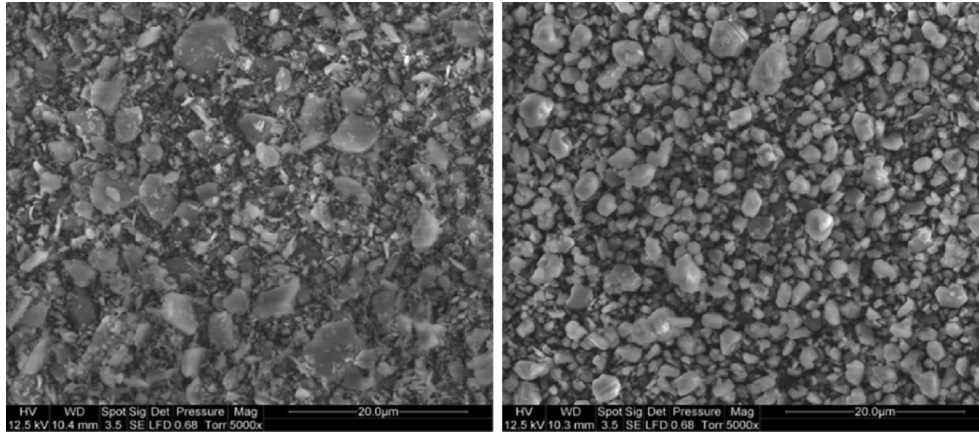
Fig. 7. Different shapes for ATH particles (left A4 − right A5).

polymer remains at the end of the cone calorimeter test.

During the cone calorimeter test, the appearance of a second peak of HRR corresponds to the cracking of the layer, noticeable on macroscopic scale. It was proposed that if the barrier is more resistant, the cracking will occur later.

Another interesting point is the relation between the time to pHRR2 (from the appearance of pHRR1) and its intensity. Later is pHRR2 (i.e. the breakdown of the barrier layer), lower is pHRR2. Fig. 11 illustrates this relation for all the formulations.

For a Δt between 300 and 500 s, the evolution of pHRR2 seems to be quite linear (formulations containing only ATH: 1 to 8). pHRR2 is reduced by 60 kW/m^2 if the peak is retarded by 100 s. Except for the formulation with only diatomite (formulation 14), composites containing synergistic agents present a later and lower pHRR2. For this category of samples, pHRR2 is reduced by 25 kW/m^2 if the peak is retarded by 100 s.

It is proposed that the resistance of the mineral layer is related to the packing of the particles. A SEM observation of the residue for a formulation exhibiting a weakly resistant barrier layer (formulation 3, containing ATH with median diameter of 10 μm) shows space between particles, and a layer apparently poorly compact. The residue of a formulation presenting a more resistant barrier layer (formulation 11, with 55% of ATH with a median diameter of 2 μm and 5% of raw diatomite), seems to be more compact, with smaller particles filling spaces between bigger ones. Images are presented on Fig. 12.
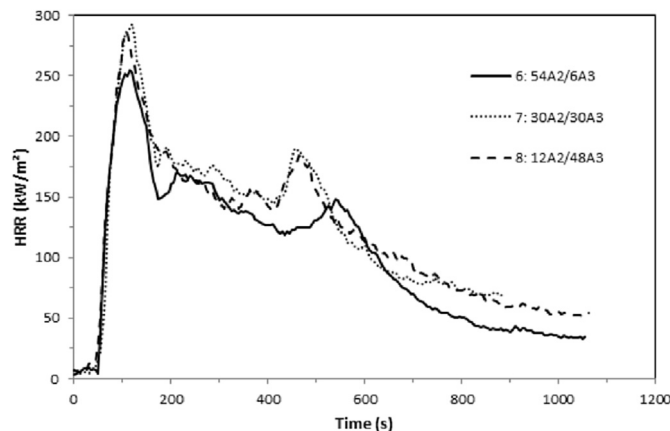
3.2. Oedometric compression results

A method to estimate the packing of particles is to proceed to an oedometric compression test, in order to measure the resistance of a layer of particles to compression. If the sample presents a higher resistance to the compression (i.e. the slope of the second part of the curve shown in Fig. 4) the packing of the particles is more efficient. For example, the compressed residue of A2 (ATH with D_{50} of 2 μm) can be easily removed from the compression cell without breaking it. Conversely, the compressed residue of A3 (ATH with D_{50} of 10 μm) collapses when removed. To analyze residues of cone calorimeter tests, a block is carefully removed, in order to have a representative sample. The slope of compressed residue of A2 is 132.14 daN and the one of A3 is 70.38 daN. Hence, the increase of the resistance to the compression is ascribed to a higher compacity of the particles in the powder bed. So, a high value of the slope may be linked to a better organization of the particles, corresponding to a supposed more cohesive barrier layer during cone calorimeter test.

Moreover, a relation was found between the compression slope of residues and the evaluation of the barrier layer resistance during cone calorimeter tests (considered as the time between pHHR1 and pHRR2), as shown in Fig. 13.

For the formulations containing only ATH (formulations 1 to 8), a residue containing fillers leading to a higher compacity of the layer of particles presents a more resistant barrier layer. The highest compression slope was measured for the residue of the formulation
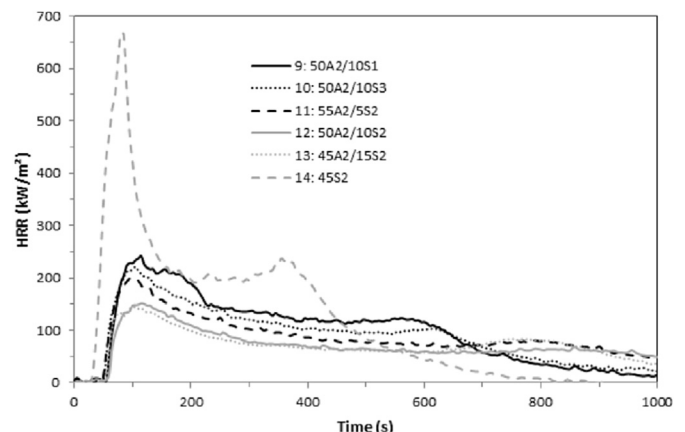

Fig. 8. HRR curves: Effect of bimodal mixtures SH100/SH20. 10%/90% (formulation 6), 50%/50% (formulation 7) and 80%/20% (formulation 8).

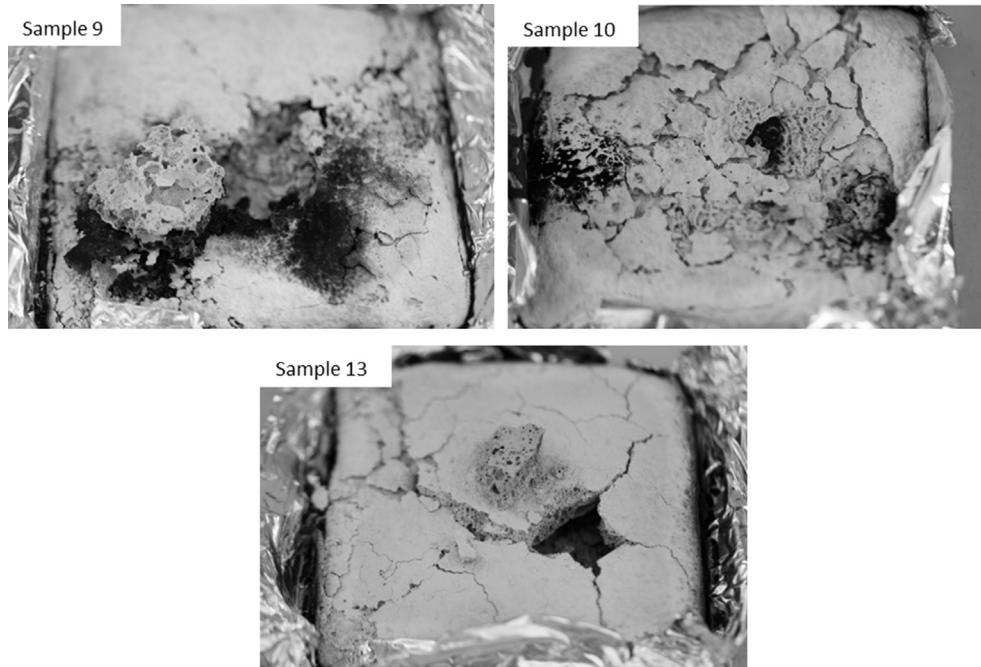**Fig. 9.** HRR curves: Presence of silica-based fillers.

Fig. 10. Residue of cone calorimeter tests of sample 9 (50A2/10S1), sample 10 (50A2/10S3) and sample 13 (45A2/15S2).

A4 (initially platelets of ATH with D_{50} of 3 μm) (147.05 daN) and corresponds to the most delayed pHRR2 (532 s between pHRR1 and pHRR2). Similarly, the lowest slope obtained with the residue of the formulation A3 (70.38 daN), corresponds to the pHRR2 with the earliest appearance (340 s after pHRR1). All other residues, containing only hydrated alumina, follow the same trend.

A different trend was noticed for the residues of formulations with silica-based agents (formulations 9 to 14). Contrary to the first ones, a lower compression slope corresponds to a more resistant barrier layer during cone calorimeter tests. On the range of values measured, the evolution seems to be linear and the barrier effect decreases when the slope of compression curves increases. A 145.02 daN slope (residue of the formulation 14: with 45% of raw diatomite) corresponds to a pHRR2 delayed by 275 s, and a 100.93 daN slope (residue of the formulation 12: with 50% of ATH and 10% of raw diatomite) corresponds to a pHRR2 delayed by

720 s. Except formulation 14, the barrier layer is more resistant for formulations containing initially not only ATH, but also a synergistic agent (i.e. the breakdown of the barrier layer occurs later in the presence of a synergistic agent). Regarding that formulation 14 is ATH-free, and that it presents a foamed structure without a significant swelling, it confirms the synergistic effect of silica-based agents used with the ATH. The silica-based agent provides the structuration of the protective layer, while the water released by the ATH seems to lead to the swelling, and so the increase of the fire retardancy of the sample.

To explain the two different trends observed, it is important to point out that residues appear slightly intumescent, like solid foam, only for composites containing synergistic agents. When the residue is not intumescent, the breakdown of the barrier layer depends on its resistance to compression.

Therefore a higher resistance to compression allows the mineral layer to maintain its integrity longer. On the contrary, when the structure is able to foam, a low resistance to compression allows a higher expansion without breaking.

Measurements of the resistance to compression for residues are quite well correlated to the breakdown of the mineral layer. However, these measurements are carried out after cone calorimeter tests and do not allow any prediction about the behaviour during the fire test. In order to attempt to predict the fire performance of EVA composites, the resistance to compression of the initial fillers (ATH and silica-based fillers before their incorporation into EVA) was measured and compared to the values obtained for the corresponding residues.

A systematic difference of 15 daN was found between the slopes of residues and these of the corresponding fillers. But a linear relation between both slopes was observed for all formulations (see Fig. 14).

Therefore it becomes possible to predict the breakdown of the barrier layer (i.e. the time and the intensity of pHRR2) from oedometric compression tests carried out on fillers before their incorporation into the matrix.
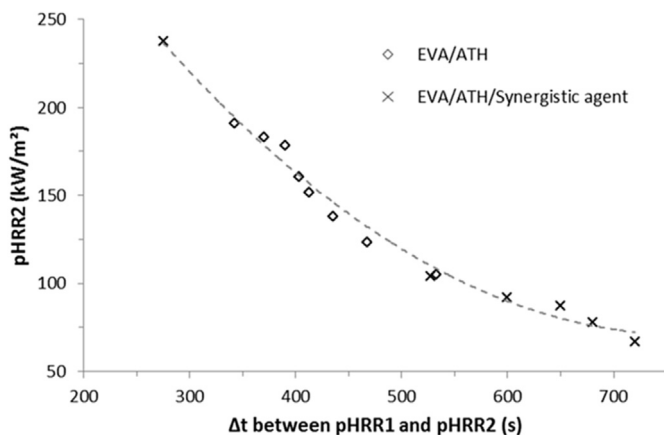

Fig. 11. Relation between the intensity of the second peak HRR and the duration between both pHRR.
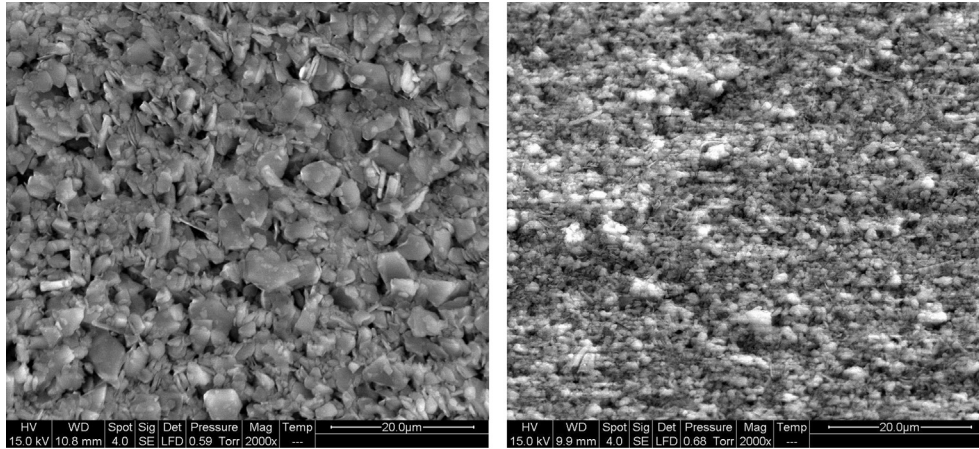
Fig. 12. Surface of the residue of formulation 3 (magnification: ×2000) and formulation 11 (magnification: ×2000).
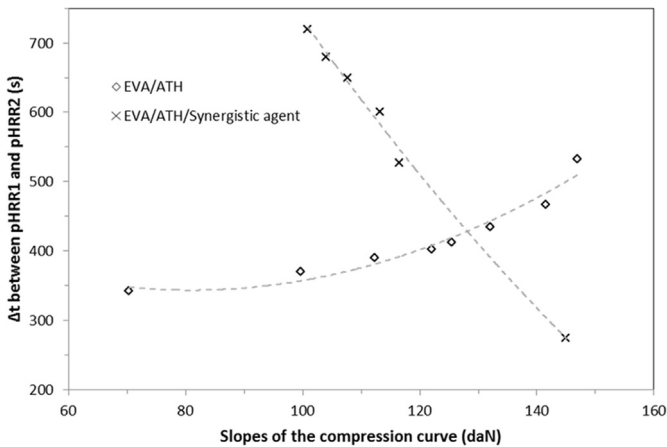

Fig. 13. Relations between the time to barrier layer breakdown during cone calorimeter tests and the slope of the compression curve for residue.

4. Conclusion

The interest of the method presented in this study is to predict and estimate the breakdown of the barrier mineral layer in EVA/ATH composites during cone calorimeter tests. Considering that the
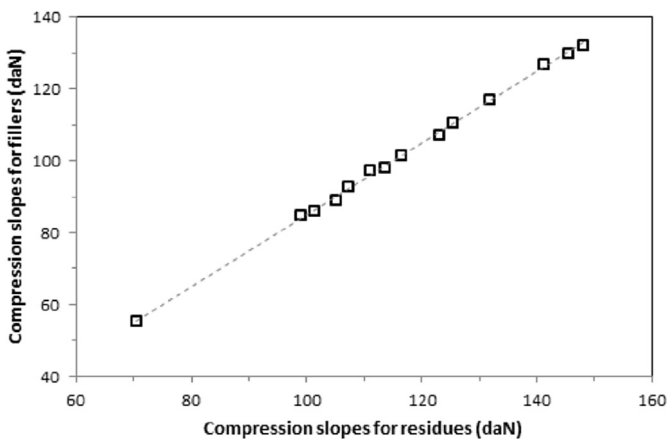

Fig. 14. Relation between slopes measured by oedometric compression for fillers and residues.

organization of particles can create a more or less compact layer, mechanical properties may be an indicator related to the resistance of this barrier.

Barrier effect was estimated by cone calorimeter, regarding the appearance of a second pHRR, related to the cracking of the layer. A relation was found between the intensity of the second pHRR and its time to appearance. So, it was shown that the barrier layer breakdown could be represented by the duration between the main pHRR and the second one.

An adapted oedometric method was used to analyze filler powders and residues of corresponding composites. The resistance to the force applied, from 0 to 10 kN, is represented by a different slope for each sample, related to the strain along the axis of compression. The results obtained with residues present a linear relation with those obtained with the corresponding fillers.

The role of the compactness of the protective layer was confirmed for composites EVA/ATH, while the breakdown of the barrier layer occurs later when the filler is more resistant to compression.

With the presence of a silica-based synergistic agent, a different trend is observed. A lower slope of compression curve corresponds to a delayed breakdown, as the composite forms an expanded structure during fire testing. The calcination of diatomite and the use of other silica-based additives allow assuming that the porous structure of the fillers influences the resistance of a structured layer. Further experiments may be carried out to confirm this observation.

Two trends were found, depending if the composite forms an expanded structure or not during fire testing. The measurement of the resistance to compression enables to estimate the appearance of the second pHRR and its intensity by analyzing the initial fillers.

This method opens up perspectives for further studies, as the influence of different shapes of particles or the optimization of mixtures of fillers for the design of more resistant barrier layers. In this article, only EVA/ATH composites were studied. Other composites will be tested to extend the method developed in this study.

Appendix A. Supplementary data

Supplementary data related to this article can be found at http://dx.doi.org/10.1016/j.polymdegradstab.2015.05.021.

References

[1] A. Henderson, Ethylene-vinyl acetate (EVA) copolymers: a general review,

Electr. Insul. Mag. 9 (1) (1993) 30–38.

[2] T.R. Hull, A. Witkowski, L. Hollingbery, Fire retardant action of mineral fillers, Polym. Degrad. Stab. 96 (8) (2011) 1462–1469.

[3] W. Zeng, N. Chen, Thermodynamic analysis of thermal decomposition of Al(OH)₃, J. Mater. Sci. Technol. 13 (1997) 446.

[4] W.E. Horn, Inorganic hydroxides and hydroxycarbonates: their function and use as flame retardants, Fire Retard Polym. Mater (2000) 285–352.

[5] J.E.J. Staggs, Modelling the effect of solid-phase additives on thermal degradation of solids, Polym. Degrad. Stab. 64 (1999) 369–377.

[6] A. Durin-France, L. Ferry, J.M. Lopez-Cuesta, A. Crespy, Magnesium hydroxide/ zinc borate/talc compositions as flame-retardants in EVA copolymer, Polym. Int. 49 (10) (2000) 1101–1105.

[7] F. Laoutid, L. Ferry, E. Leroy, J.M. Lopez-Cuesta, Intumescent mineral fire retardant systems in ethylene–vinyl acetate copolymer: effect of silica particles on char cohesion, Polym. Degrad. Stab. 91 (9) (2006) 2140–2145.

[8] N.D. Zaharri, N. Othman, Z.A.M. Ishak, Thermal and mechanical properties of zeolite filled Ethylene vinyl acetate composites, Proced. Chem. 4 (2012) 95–100.

[9] M. Batistella, B. Otazaghine, R. Sonnier, A.S. Caro-Bretelle, C. Petter, J.M. Lopez-Cuesta, Fire retardancy of ethylene vinyl acetate/ultrafine kaolinite composites, Polym. Degrad. Stab. 100 (2014) 54–62.

[10] R.P. Dias, J.A. Teixeira, M.G. Mota, A.I. Yelshin, Particulate binary mixtures: dependence of packing porosity on particle size ratio, Indust Eng. Chem. Res. 43 (24) (2004) 7912–7919.

[11] M.A. Cárdenas, D. García-López, I. Gobernado-Mitre, J.C. Merino, J.M. Pastor, J.D.D. Martínez, J. Barbeta, D. Calveras, Mechanical and fire retardant properties of EVA/clay/ATH nanocomposites: effect of particle size and surface treatment of ATH filler, Polym. Degrad. Stab. 93 (11) (2008) 2032–2037.

[12] L. Tibiletti, C. Longuet, L. Ferry, P. Coutelen, A. Mas, J.J. Robin, J.M. Lopez-Cuesta, Thermal degradation and fire behaviour of unsaturated polyesters filled with metallic oxides, Polym. Degrad. Stab. 96 (1) (2011) 67–75.

[13] J.C. Benezet, P. Adamiec, M. Nemoz-Gaillard, Study of real granular assemblies, Powder Technol. 173 (2) (2007) 118–125.

[14] K. Han, Y.T. Feng, D.R.J. Owen, Sphere packing with a geometric based compression algorithm, Powder Technol. 155 (1) (2005) 33–41.

[15] J.M. Montes, F.G. Cuevas, J. Cintas, Effective area in powder compacts under uniaxial compression, Mater. Sci. Eng. 395 (2005) 208–213.

[16] F.Y. Hshieh, Shielding effects of silica-ash layer on the combustion of silicones and their possible applications on the fire retardancy of organic polymers, Fire Mater. 22 (2) (1998) 69–76.

[17] Y.M. Reznik, Engineering approach to interpretation of oedometer tests performed on collapsible soils, Eng. Geol. 57 (2000) 205–213.

[18] J.P. Magnan, C. Mieussens, B. Soyez, J. Vautrain, Essais Oedométriques: Méthodes D'essai LPC, 13, 1985, p. 83.

[19] B. Schartel, M. Bartholmai, U. Braun, Barrier Effects for the Fire Retardancy of Polymers, in: Fire Retard Polymers: New Appl Miner Fillers, 2005, pp. 264–275.

[20] N. Ediz, İ. Bentli, İ. Tatar, Improvement in filtration characteristics of diatomite by calcination, Int. J. Min. Process 94 (3–4) (2010) 129–134.

[21] R. Rothon, P. Hornsby, Fire retardant fillers for polymers, Polym. Green. Flame Retard. (2014) 289–321.

[22] R.N. Rothon, P.R. Hornsby, Flame retardant effects of magnesium hydroxide, Polym. Degrad. Stab. 54 (1996) 383–385.

[23] F. Akhtar, Y. Rehman, L. Bergström, A study of the sintering of diatomaceous earth to produce porous ceramic monoliths with bimodal porosity and high strength, Powder Technol. 201 (3) (2010) 253–257.